

Lateral Josephson effect on the surface of $\text{Co}_3\text{Sn}_2\text{S}_2$ magnetic Weyl semimetal

O.O. Shvetsov, V.D. Esin, Yu.S. Barash, A.V. Timonina, N.N. Kolesnikov, and E.V. Deviatov

*Institute of Solid State Physics of the Russian Academy of Sciences,
Chernogolovka, Moscow District, 2 Academician Ossipyan str., 142432 Russia*

(Dated: January 27, 2020)

We experimentally study lateral electron transport between two $5\ \mu\text{m}$ spaced superconducting indium leads on a top of magnetic Weyl semimetal $\text{Co}_3\text{Sn}_2\text{S}_2$. For the disordered magnetic state of $\text{Co}_3\text{Sn}_2\text{S}_2$ crystal, we only observe the Andreev reflection in the proximity of each of the leads, which is indicative of highly transparent In- $\text{Co}_3\text{Sn}_2\text{S}_2$ interfaces. If the sample is homogeneously magnetized, it demonstrates well-developed anomalous Hall effect state. In this regime we find the Josephson current that takes place even for $5\ \mu\text{m}$ long junctions and shows the unusual magnetic field and temperature dependencies. As a possible reason for the results obtained, we discuss the contribution to the proximity-induced spin-triplet Josephson current from the topologically protected Fermi-arc states on the surface of $\text{Co}_3\text{Sn}_2\text{S}_2$.

PACS numbers: 73.40.Qv 71.30.+h

I. INTRODUCTION

Similarly to topological insulators¹ and quantum Hall systems^{2,3}, Weyl semimetals^{4,5} (WSM) have topologically protected surface states. They are Fermi arcs connecting projections of Weyl nodes on the surface Brillouin zone and these surface states inherit the chiral property of the Chern insulator edge states⁵. WSMs should have either space-inversion or time-inversion symmetry to be broken. First experimentally investigated WSMs were non-centrosymmetric crystals, where spin- and angle-resolved photoemission spectroscopy data have demonstrated spin-polarized surface Fermi arcs^{6,7}.

There are only a few candidates of magnetically ordered materials^{4,8–10} for the realization of WSMs in the systems with broken time reversal symmetry. Recently, giant anomalous Hall effect (AHE) was reported^{11,12} for the kagome-lattice ferromagnet $\text{Co}_3\text{Sn}_2\text{S}_2$ as an anomalous Hall conductance in zero magnetic field. The AHE can be regarded as the indication to a magnetic Weyl phase⁵, as supported by the topological-insulator-multilayer model, where the two-dimensional Chern edge states form the three-dimensional WSM surface states¹³. The Fermi arc surface states, indeed, were directly visualized in $\text{Co}_3\text{Sn}_2\text{S}_2$ by scanning tunneling spectroscopy¹⁴.

For normal metals, Andreev reflection¹⁵ allows charge transport from the metal (N) to superconductor (S) through the NS interface by creating a Cooper pair at energies below the superconducting gap^{15,16}. For two closely spaced superconducting leads, i.e. for the SNS junction, multiple Andreev reflection can contribute to the subharmonic structure of the current-voltage characteristics^{16,17}.

For topological materials, the proximity to a superconductor usually demonstrates non-trivial physics^{18–20}. As it was experimentally shown, the Josephson coupling in a topological insulator is established through the surface conducting channels²¹. The edge current contribution can be retrieved even for systems with conducting bulk by analyzing the Josephson current behavior^{22–24}.

In Weyl semimetals, various topological superconducting states can appear^{25–28} and various types of Andreev reflection can take place^{28,29}, depending on the particular conditions. Thus the specular Andreev reflection, reminiscent the one in the graphene^{30,31}, can take place at the Weyl semimetal - Weyl superconductor interface²⁹, while the chirality blockade of Andreev reflection can appear at the interface of the magnetic Weyl semimetal and the conventional s-wave spin-singlet superconductor²⁸.

For magnetically ordered topological materials the proximity to a superconductor is a new and emerging field involving the mutual influence of superconductivity and magnetism under nontrivial topological conditions, e.g., in the presence of topologically protected interface states. For example, it has been theoretically identified that the proximity to a superconductor can result in the Majorana modes originating from the Fermi arc in a Weyl semimetal wire with an axial magnetization³². It has also been predicted³³, that the proximity induced superconducting surface states of magnetically doped topological insulators can represent chiral Majorana modes. Thus, it is reasonable to study proximity effects in superconducting junctions, fabricated on a three-dimensional magnetic Weyl semimetal surface.

Here, we experimentally study lateral electron transport between two $5\ \mu\text{m}$ spaced superconducting indium leads on a top of magnetic Weyl semimetal $\text{Co}_3\text{Sn}_2\text{S}_2$. For the disordered magnetic state of $\text{Co}_3\text{Sn}_2\text{S}_2$ crystal, we only observe the Andreev reflection in the proximity of each of the leads, which is indicative of highly transparent In- $\text{Co}_3\text{Sn}_2\text{S}_2$ interfaces. If the sample is homogeneously magnetized, it demonstrates well-developed anomalous Hall effect state. In this regime we find the Josephson current that takes place even for $5\ \mu\text{m}$ long junctions and shows the unusual magnetic field and temperature dependencies. As a possible reason for the results obtained, we discuss the contribution to the proximity-induced spin-triplet Josephson current from the topologically protected Fermi-arc states on the surface of $\text{Co}_3\text{Sn}_2\text{S}_2$.

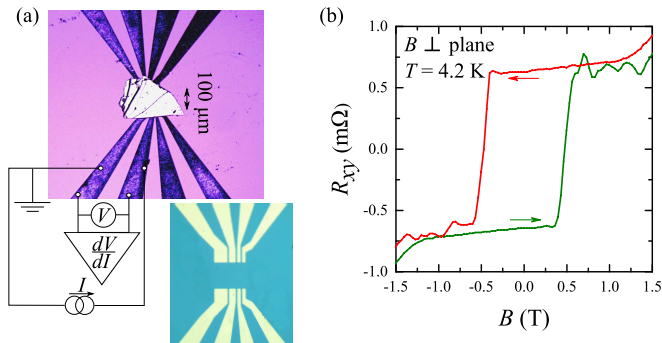


FIG. 1. (Color online) (a) A top-view image of the sample with the sketch of electrical connections. A flat (about $100 \mu\text{m}$ size and $1 \mu\text{m}$ thick) single-crystal $\text{Co}_3\text{Sn}_2\text{S}_2$ flake is weakly pressed on the insulating SiO_2 substrate with 100 nm thick, $5 \mu\text{m}$ separated In leads. The leads pattern is demonstrated in the bottom image. Non-linear $dV/dI(I)$ curves are measured by a standard four-point technique, all the wire resistances are excluded. (b) Giant anomalous Hall effect, which confirms high quality of our $\text{Co}_3\text{Sn}_2\text{S}_2$ samples^{11,12}. Arrows indicate the field scanning directions.

II. SAMPLES AND TECHNIQUE

$\text{Co}_3\text{Sn}_2\text{S}_2$ single crystals were grown by the gradient freezing method. Initial load of high-purity elements taken in stoichiometric ratio was slowly heated up to 920°C in the horizontally positioned evacuated silica ampule, held for 20 h and then cooled with the furnace to the ambient temperature at the rate of 20 deg/h . The obtained ingot was cleaved in the middle part. The Laue patterns confirm the hexagonal structure with (0001) as cleavage plane. Electron probe microanalysis of cleaved surfaces and X-ray diffractometry of powdered samples confirmed stoichiometric composition of the crystal.

Weyl semimetals are essentially three-dimensional⁵ macroscopic crystals. Despite it is possible to form contacts directly on the polished crystal plane, we use another technique, which is known to provide highly transparent contacts^{20,24,34}. The leads pattern is formed on the insulating SiO_2 substrate by lift-off technique after thermal evaporation of 100 nm In, see Fig. 1 (a). The indium leads are separated by $5 \mu\text{m}$ intervals. Since the kagome-lattice ferromagnet $\text{Co}_3\text{Sn}_2\text{S}_2$ can be easily cleaved along (0001) crystal plane, small (about $100 \mu\text{m}$ size and $1 \mu\text{m}$ thick) $\text{Co}_3\text{Sn}_2\text{S}_2$ flakes are obtained by a mechanical cleaving method. Then we select the most plane-parallel flakes with clean surface, where no surface defects could be resolved with optical microscope. They are transferred to the In leads pattern and pressed slightly with another oxidized silicon substrate. A special metallic frame allows us to keep the substrates parallel and apply a weak pressure to the sample. No external pressure is needed for a $\text{Co}_3\text{Sn}_2\text{S}_2$ flake to hold on to a substrate with In leads afterward. This procedure provides transparent contacts, stable in different cooling cycles, which has been also demonstrated before^{20,24,34}.

Magnetoresistance measurements confirms high quality of the prepared $\text{Co}_3\text{Sn}_2\text{S}_2$ samples. We check that samples demonstrate giant anomalous Hall effect, as it has been previously reported^{11,12} for $\text{Co}_3\text{Sn}_2\text{S}_2$ semimetal. Fig. 1 (b) shows hysteresis behavior and sharp switchings in Hall resistance R_{xy} , the switchings' positions $\approx 0.5 \text{ T}$ even quantitatively coincide with the reported values^{11,12}. According to our sample dimensions, the Hall resistivity ρ_{xy} can be estimated as $1 \mu\Omega\text{cm}$ in zero magnetic field, which is three times smaller in comparison with Refs.^{11,12}.

We study electron transport between two $5 \mu\text{m}$ separated In leads by a standard four-point technique. The principal circuit diagram is depicted in Fig. 1 (a). In this connection scheme, all the wire resistances are excluded, which is necessary for low-impedance In- $\text{Co}_3\text{Sn}_2\text{S}_2$ -In junctions. To obtain $dV/dI(I)$ characteristics, the dc current I (up to 1 mA) is additionally modulated by a low ($\approx 5 \mu\text{A}$) ac component. We measure both dc (V) and ac (which is proportional to dV/dI) components of the voltage drop with a dc voltmeter and a lock-in, respectively, after a broad-band preamplifier. The measurements are performed in a dilution refrigerator for the temperature interval $30 \text{ mK} - 1.2 \text{ K}$.

If the SNS junction demonstrates zero resistance, an important information can be obtained²²⁻²⁴ from the maximum supercurrent I_c suppression by temperature T and magnetic field B . To obtain I_c values with high accuracy for given (B, T) values, we sweep current I ten times from zero value (superconducting $dV/dI = 0$ state) to some value well above the I_c (i.e. to the resistive $dV/dI > 0$ state), and then determine I_c as an average value of $dV/dI = 0$ breakdown positions in different sweeps.

III. EXPERIMENTAL RESULTS

$\text{Co}_3\text{Sn}_2\text{S}_2$ magnetic properties arise from the kagome-lattice cobalt planes, whose magnetic moments order ferromagnetically¹¹ out of plane below 175 K . Since the samples are cooled down from room temperature in zero magnetic field, the initial state of a macroscopic $\text{Co}_3\text{Sn}_2\text{S}_2$ flake is magnetically disordered one, e.g., due to magnetic domains. The size of these domains is typically around the order of a micrometer³⁵ in $\text{Co}_3\text{Sn}_2\text{S}_2$, which is much smaller than the distance between the indium leads in our samples. To obtain a definite AHE state of magnetically ordered WSM, the magnetization procedure is performed: an external magnetic field is swept slowly from -1.5 T to $+1.5 \text{ T}$, both limits are far above the switching positions in Fig. 1 (b). Afterward, the external field goes down to zero.

Examples of $dV/dI(I)$ characteristics are shown in Fig. 2 (a) and (b) before and after the magnetization procedure, respectively, for the same sample in a single cooling cycle.

Before magnetization, the curves demonstrate well

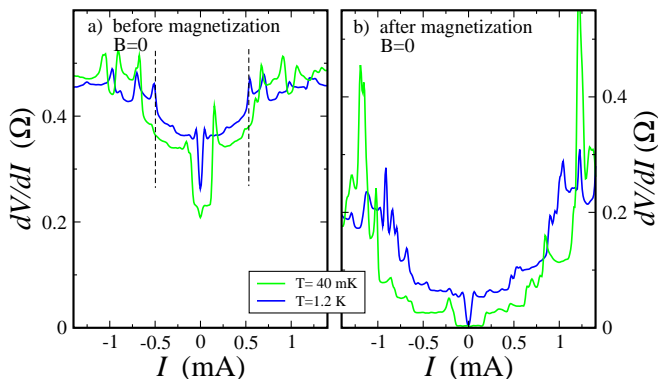


FIG. 2. (Color online) Examples of $dV/dI(I)$ curves before sample magnetization (a) and after it (b), for the same sample in a single cooling cycle. Diminishing the temperature from 1.2 K to 40 mK has low effect on the initial Andreev-like $dV/dI(I)$ curves in (a). Dashed lines indicate the wide dV/dI resistance drop in (a), caused by Andreev reflection. In contrast, the magnetization procedure transforms $dV/dI(I)$ curves into the Josephson-like ones in (b). The width of a wide zero-resistance region depends on the temperature below 1.2 K. The data are obtained in zero magnetic field.

known Andreev behavior. Since Andreev reflection allows subgap transport of Cooper pairs, it appears experimentally as the resistance drop for voltages within the superconducting gap¹⁶. As it can be seen in Fig. 2 (a), differential resistance is diminished within $\approx \pm 0.5$ mA bias interval in respect to the normal resistance value $\approx 0.5\Omega$. The superconducting gap can be estimated from the width of this region as $0.5 \text{ mA} \times 0.5 \Omega \approx 0.25 \text{ meV}$. Since the bulk indium is known³⁶ to have the 0.5 meV gap, the obtained value is quite reasonable for the indium film on a top of a ferromagnet. Temperature has low effect on $dV/dI(I)$ curves, even at 40 mK the minimal resistance is not below one half of the normal value, see Fig. 2 (a).

The magnetization procedure changes the $dV/dI(I)$ curves dramatically, see Fig. 2 (b): the zero-bias resistance value drops to zero. At low temperature of 40 mK, we observe a definite zero-resistance state in a wide current region, which qualitatively resembles the Josephson effect¹⁶. This behavior has been checked to be independent of the value and sign of the magnetization field.

As it is expected for the Josephson effect, the zero-resistance state can be suppressed by magnetic field. Even at the highest temperature, the junction resistance is zero in a finite, ± 1 mT field interval, see Fig. 3 (a). This behavior is demonstrated in detail in Fig. 3 (b) for $dV/dI(I)$ curves at lowest temperature of 40 mK. The zero-resistance state survives up to 3.2 mT. Above 3.2 mT field, $dV/dI(I)$ curves demonstrate usual Andreev behavior, because the indium leads are still superconducting below the critical indium field³⁷ of about 40 mT.

Thus, we demonstrate in Figs. 2 and 3, that two superconducting contacts induce Josephson current in an

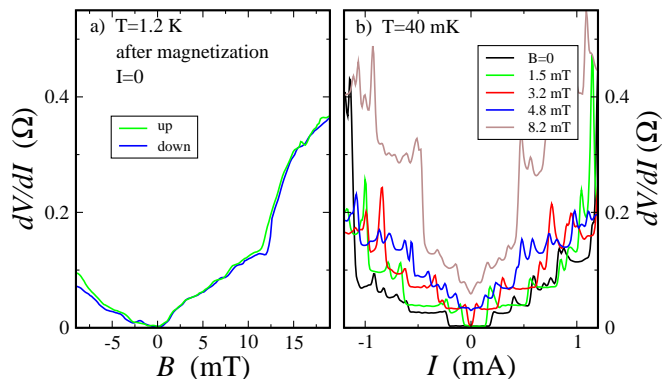


FIG. 3. (Color online) Suppression of the zero-resistance state by magnetic field. (a) Differential resistance dV/dI at zero dc current as a function of magnetic field. A finite zero-resistance region can be seen even at highest, 1.2 K, temperature. Two curves correspond to the opposite field sweep directions, they do not strictly coincide in the normal state. (b) Examples of $dV/dI(I)$ characteristics for different magnetic fields at 40 mK. The zero-resistance region survives above 3.2 mT at this temperature. The magnetic field is perpendicular to the flake's plane. The sample is the same as in Fig. 2 (after magnetization).

unprecedentedly long $L = 5 \mu\text{m}$ In-Co₃Sn₂S₂-In junction. The above described behavior can be reproduced for different samples, see, e.g., Fig. 4. In this case, the normal dV/dI resistance is one order higher, about 3 Ohm, as depicted in the main field in Fig. 4 (a). The differential resistance is diminished within ± 0.075 mA interval, which gives the same $0.075 \text{ mA} \times 3 \Omega \approx 0.25 \text{ meV}$ superconducting gap value. Before sample magnetization, dV/dI is always finite even at 40 mK, see Fig. 4 (a), while it drops to zero after the magnetization procedure.

We also observe unusual behavior of the temperature and magnetic field dependences of the critical current I_c . Lower currents are more suitable for accurate determination of I_c , so the results are presented in the insets to Fig. 4 (a) and (b). All the experimental points are well reproducible, variation of I_c in different sweeps is below the symbol size in the inset.

$I_c(T)$ demonstrates weak temperature dependence below 0.75 K, while I_c is diminishing strongly above it to one half of the initial value at our highest 1.2 K, see the inset to Fig. 4 (a). This dependence can be crudely extrapolated to ≈ 2 K critical temperature, which well correspond to the 0.25 meV superconducting gap, determined from the Andreev curve in Fig. 4 (a). However, $I_c(T)$ does not demonstrate the conventional for long diffusive SNS junctions exponential decay^{38,39}. The experimental $I_c(T)$ resemble the results for Josephson junctions with spin-flip scattering⁴⁰.

The zero-resistance state at $I = 0$ is suppressed by magnetic field at ± 7 mT, see Fig. 4 (b). The full $I_c(B)$ pattern is depicted in the inset to Fig. 4 (b). At lowest temperatures, $I_c(B)$ is changing very slowly (within 10%) until ± 7 mT, but falls to zero above this value. The char-

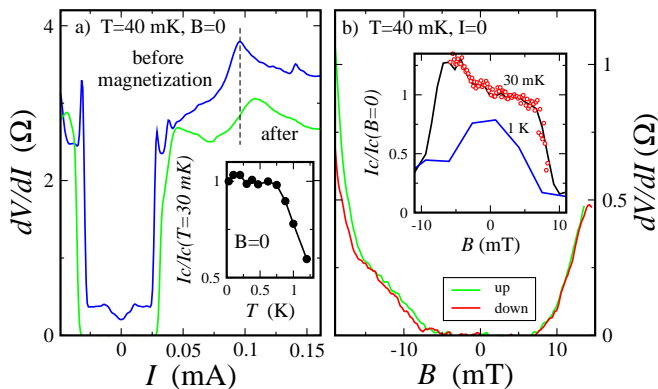


FIG. 4. (Color online) Experimental results for a different sample at minimal 40 mK temperature. (a) Formation of the Josephson-type curve (the green one) with well-defined critical current (about 0.025 mA) after sample magnetization. Dashed line indicates the superconductive gap position for the Andreev-like curve (the blue one) without zero-resistance state. Inset demonstrates temperature dependence of the critical current, which is unusual for long diffusive Josephson junctions. (b) Suppression of the zero-resistance state by magnetic field at zero dc current for two opposite field sweep directions. Inset demonstrates critical current as a function of magnetic field for two different temperatures. At 40 mK, the $I_c(B)$ is antisymmetric in respect to the zero field, but symmetrically falls to zero at ± 7 mT. The antisymmetry is confirmed by extremely slow field sweep with a low step, as demonstrated by open circles. The expected $I_c(B)$ symmetry is restored above 1 K. The magnetic field is perpendicular to the flake's plane.

acteristic feature is that the low-field $I_c(B)$ dependence is antisymmetric in respect to the zero field. This behavior is confirmed by extremely slow field sweep with a large amount of points, as demonstrated by open circles in the inset. There are also some $I_c(B)$ oscillations within the ± 7 mT interval. Both the antisymmetry and the oscillations are destroyed by temperature above 0.75 K. The shallow oscillations in $I_c(B)$ could be related with usual interference effects¹⁶, although the corresponding curve substantially differs from the standard Fraunhofer pattern⁴¹ and no strong suppression of $I_c(B)$ at $B < \pm 7$ mT is observed.

It is important, that both for the resistance at $I = 0$ in the main Fig. 4 (b) and for significant current ≈ 0.05 mA in the inset, the Josephson effect is destroyed under the same magnetic fields ± 7 mT. Thus, there is no sample overheat in $I_c(B, T)$ measurements, so the unusual $I_c(T)$ temperature dependence is correct in the inset to Fig. 4 (a).

IV. DISCUSSION

As a result, we demonstrate Josephson current through the magnetically ordered $5\mu\text{m}$ long In- $\text{Co}_3\text{Sn}_2\text{S}_2$ -In junctions, where $\text{Co}_3\text{Sn}_2\text{S}_2$ flake is in a definite AHE state.

On the other hand, no supercurrent can be observed in these junctions, when $\text{Co}_3\text{Sn}_2\text{S}_2$ is in the disordered magnetic state. This effect is well reproducible for different samples, see Figs. 2 and 4 (a).

First of all, we should exclude possible fabrication defects, like unintentional shunt connections in the junction's plane. The crucial argument against the presence of any leakage is a pronounced dependence of the Josephson effect on the WSM magnetization. For conventional superconductors like indium, the proximity to a ferromagnet weakens superconductivity. Just opposite to the known indium behavior, magnetically ordered state of $\text{Co}_3\text{Sn}_2\text{S}_2$ enhances the Josephson coupling. Also, the thickness of the indium film is chosen to be much smaller than the leads separation ($100\text{ nm} \ll 5\mu\text{m}$) to avoid shorting of In leads when pressing the $\text{Co}_3\text{Sn}_2\text{S}_2$ flake.

Thus, one can be sure that the observed Josephson current flows through the proximity-influenced magnetically ordered $\text{Co}_3\text{Sn}_2\text{S}_2$ WSM.

The surface states transport can be a key point to explain our experimental results. In the case of $\text{Co}_3\text{Sn}_2\text{S}_2$, Fermi-arc surface states have been directly identified by scanning tunneling spectroscopy¹⁴. The giant anomalous Hall effect is interpreted in terms of the surface states⁵, and we observe the Josephson effect only after magnetization procedure, i.e. for a well pronounced AHE state, see Fig. 1 (b). Therefore, Weyl surface states exist along the macroscopic $\text{Co}_3\text{Sn}_2\text{S}_2$ flake. Their proximity-induced pairing results in the effective supercurrent-carrying channels. The important role of the chiral surface channels in the Josephson transport studied is also supported by their topological protection and the lateral geometry of the junction.

The magnetic domain structure in $\text{Co}_3\text{Sn}_2\text{S}_2$ flake can have a substantial influence on the junction's properties. When the domain magnetization in the $\text{Co}_3\text{Sn}_2\text{S}_2$ sample is disordered just after the sample cooling, the chirality of Weyl nodes can switch across the magnetic domain walls⁵ and a continuous surface state can only appear along a single magnetic domain, which size is around the order of a micrometer³⁵. Such a disordered magnetic structure should produce significant disordered spin-flip processes and can prevent the Josephson effect to develop between the $5\mu\text{m}$ spaced indium leads, allowing only the observation of Andreev reflection in the proximity of each of the leads, in accordance with our measurements for samples before the magnetization procedure.

Since the Weyl surface states are spin-polarized^{5,14,42} and $\text{Co}_3\text{Sn}_2\text{S}_2$ itself is a half-metal⁴², one can expect a triplet supercurrent⁴³⁻⁴⁵ through $\text{Co}_3\text{Sn}_2\text{S}_2$. When singlet Cooper pairs from the superconductor are converted into triplet pairs within the spin-polarized material, a long-range proximity effect, as known, can take place: while the singlet component penetrates into the ferromagnet over a short length⁴⁶ $\xi_h = (\hbar D/E_{ex})^{1/2}$ (E_{ex} is the exchange energy and D is the diffusion coefficient), the triplet component penetrates over a much longer length $(\hbar D/k_B T)^{1/2}$, which is of the same order

as that for the penetration of the superconducting pairs into a normal metal⁴³. This conclusion prohibits, in particular, the conventional long-range s-wave spin-singlet pairing in $\text{Co}_3\text{Sn}_2\text{S}_2$ flake, which occurs in In and cannot be present in the magnetic Weyl semimetal, as also follows from the chirality blockade arguments²⁸. Since the exchange field and spin-orbit coupling are jointly present in Weyl semimetals, the singlet-triplet conversion at its interface does not require additional magnetic inhomogeneities^{47,48}.

The triplet supercurrent can be responsible for the low-field $I_c(B)$ antisymmetry in the inset to Fig. 4 (b). While in topological insulators the surface conducting channels have been experimentally identified as dominating in establishing the Josephson coupling²¹, the Josephson current in Weyl semimetals can be transferred generally via both the surface and the bulk channels⁴⁹. The low-field variation of $I_c(B)$ reflects the magnetization dynamics in the bulk $\text{Co}_3\text{Sn}_2\text{S}_2$, since in the inset to Fig. 4 (b) I_c is smaller for positive fields and for positively magnetized flake. As opposed to the low-field region, the fields exceeding $B_c \approx \pm 7$ mT can be considered as destroying the superconducting pairing via the surface channels, where the topologically protected magnetic ordering is not sensitive to the lower values of the external field. We wish to mention that uneven indium contact spacing may distort the behavior of $I_c(B)$. For example, it (partly) suppresses the Fraunhofer pattern⁴¹. However, it can not make $I_c(B)$ to be sensitive to the sign of the magnetic

field, which we observe as the low-field antisymmetry.

V. CONCLUSION

As a conclusion, we experimentally study lateral electron transport between two $5 \mu\text{m}$ spaced superconducting indium leads on a top of magnetic Weyl semimetal $\text{Co}_3\text{Sn}_2\text{S}_2$. For the disordered magnetic state of $\text{Co}_3\text{Sn}_2\text{S}_2$ crystal, we only observe the Andreev reflection in the proximity of each of the leads, which is indicative of highly transparent In- $\text{Co}_3\text{Sn}_2\text{S}_2$ interfaces. If the sample is homogeneously magnetized, it demonstrates well-developed anomalous Hall effect state. In this regime we find the Josephson current that takes place even for $5 \mu\text{m}$ long junctions and shows the unusual magnetic field and temperature dependencies. As a possible reason for the results obtained, we discuss the contribution to the proximity-induced spin-triplet Josephson current from the topologically protected Fermi-arc states on the surface of $\text{Co}_3\text{Sn}_2\text{S}_2$.

ACKNOWLEDGMENTS

We wish to thank V.T. Dolgoplov for fruitful discussions, and S.V. Simonov for X-ray sample characterization. We gratefully acknowledge financial support partially by the RFBR (project No. 19-02-00203), RAS, and RF State task.

-
- ¹ M. Z. Hasan and C. L. Kane, *Rev. Mod. Phys.* **82**, 3045 (2010).
- ² M. Büttiker, *Phys. Rev. B* **38**, 9375 (1988).
- ³ E. V. Deviatov, *Physics-Uspexhi* **50** (2) 197 (2007).
- ⁴ X. Wan, A. M. Turner, A. Vishwanath, S. Y. Savrasov, *Phys. Rev. B* **83**, 205101 (2011).
- ⁵ For a review on topological semimetals, see N.P. Armitage, E.J. Mele, and A. Vishwanath, *Rev. Mod. Phys.* **90**, 015001 (2018).
- ⁶ P.K. Das, D.D. Sante, I. Vobornik, J. Fujii, T. Okuda, E. Bruyer, A. Gyenis, B.E. Feldman, J. Tao, R. Ciancio, G. Rossi, M.N. Ali, S. Picozzi, A. Yazdani, G. Panaccione, and R.J. Cava, *Nature Comm.* **7**, 10847 (2016).
- ⁷ B. Feng, Y.-H. Chan, Y. Feng, R.-Y. Liu, M.-Y. Chou, K. Kuroda, K. Yaji, A. Harasawa, P. Moras, A. Barinov, W. Malaeb, C. Bareille, T. Kondo, S. Shin, F. Komori, T.-C. Chiang, Y. Shi, and I. Matsuda, *Phys Rev B* **94**, 195134 (2016).
- ⁸ M. Hirschberger, S. Kushwaha, Z. Wang, Q. Gibson, S. Liang, C. A. Belvin, B. A. Bernevig, R. J. Cava, N. P. Ong, *Nat. Mater.* **15**, 1161-1165 (2016).
- ⁹ G. Xu, H. Weng, Z. Wang, X. Dai, Z. Fang, *Phys. Rev. Lett.* **107**, 186806 (2011).
- ¹⁰ S. K. Kushwaha, Z. Wang, T. Kong, R. J. Cava, *J. Phys. Condens. Matter.* **30**, 075701 (2018).
- ¹¹ Enke Liu, Yan Sun, Nitesh Kumar, Lukas Muechler, Aili Sun, Lin Jiao, Shuo-Ying Yang, Defa Liu, Aiji Liang, Qiunan Xu, Johannes Kroder, Vicky Süß, Horst Borrmann, Chandra Shekhar, Zhaosheng Wang, Chuanying Xi, Wenhong Wang, Walter Schnelle, Steffen Wirth, Yulin Chen, Sebastian T. B. Goennenwein, and Claudia Felser, *Nature Physics* **14**, 1125 (2018).
- ¹² Qi Wang, Yuanfeng Xu, Rui Lou, Zhonghao Liu, Man Li, Yaobo Huang, Dawei Shen, Hongming Weng, Shancai Wang and Hechang Lei, *Nature Communications* **9**, 3681 (2018).
- ¹³ A. A. Burkov, Leon Balents, *Phys. Rev. Lett.* **107**, 127205 (2011).
- ¹⁴ Noam Morali, Rajib Batabyal, Pranab Kumar Nag, Enke Liu, Qiunan Xu, Yan Sun, Binghai Yan, Claudia Felser, Nurit Avraham, Haim Beidenkopf, arXiv:1903.00509
- ¹⁵ A. F. Andreev, *Soviet Physics JETP* **19**, 1228 (1964).
- ¹⁶ M. Tinkham, *Introduction to Superconductivity* (2d ed., McGrawHill, New York, 1996).
- ¹⁷ N. Agrait, A. Levy Yeyati, and J. M. van Ruitenbeek, *Phys. Rep.* **377**, 81 (2003).
- ¹⁸ L. Fu and C. L. Kane, *Phys. Rev. Lett.* **100**, 96407 (2008).
- ¹⁹ A. Kononov, V.A. Kostarev, B.R. Semyagin, V.V. Preobrazhenskii, M.A. Putyato, E.A. Emelyanov, and E.V. Deviatov, *Physical Review B* **96**, 245304 (2017). DOI: 10.1103/PhysRevB.96.245304

- ²⁰ A. Kononov, O.O. Shvetsov, S.V. Egorov, A.V. Timonina, N.N. Kolesnikov and E.V. Deviatov EPL, 122, 27004 (2018)
- ²¹ Jae Hyeong Lee, Gil-Ho Lee, Joonbum Park, Janghee Lee, Seung-Geol Nam, Yun-Sok Shin, Jun Sung Kim, and Hu-Jong Lee Nano Letters, 14(9), 50295034 (2014). <http://doi.org/10.1021/nl501481b>
- ²² Sean Hart, Hechen Ren, Timo Wagner, Philipp Leubner, Mathias Mhlbauer, Christoph Brne, Hartmut Buhmann, Laurens W. Molenkamp & Amir Yacoby, Nature Physics 10, 638643 (2014), doi:10.1038/nphys3036
- ²³ Vlad S. Pribiag, Arjan J. A. Beukman, Fanming Qu, Maja C. Cassidy, Christophe Charpentier, Werner Wegscheider & Leo P. Kouwenhoven, Nature Nanotechnology 10, 593 (2015)
- ²⁴ O.O. Shvetsov, A. Kononov, A.V. Timonina, N.N. Kolesnikov, E.V. Deviatov, JETP Letters, 107, 774779 (2018); EPL, 124, 47003 (2018).
- ²⁵ T. Meng and L. Balents, Phys. Rev. B 86, 054504 (2012).
- ²⁶ G. Y. Cho, J. H. Bardarson, Y.-M. Lu, and J. E. Moore, Phys. Rev. B 86, 214514 (2012).
- ²⁷ H. Wei, S. P. Chao, and V. Aji, Phys. Rev. B 89, 014506 (2014).
- ²⁸ N. Bovenzi, M. Breitzkreiz, P. Baireuther, T. E. OBrien, J. Tworzydo, I. Adagideli, and C. W. J. Beenakker, Phys. Rev. B 96, 035437 (2017).
- ²⁹ Wei Chen, Liang Jiang, R. Shen, L. Sheng, B. G. Wang, D. Y. Xing EPL 103, 27006 (2013).
- ³⁰ C. W. J. Beenakker, Physical Review Letters 97, 067007 (2006).
- ³¹ C. W. J. Beenakker, Reviews of Modern Physics 80, 1337 (2008).
- ³² P Baireuther, J Tworzydlo, M Breitzkreiz, I Adagideli and CW J Beenakker, New J. Phys. 19, 025006 (2017).
- ³³ Tsubasa Toki, Sho Nakosai, Yukio Tanaka, Yuki Kawaguchi, arXiv:1906.01934
- ³⁴ O. O. Shvetsov, V. D. Esin, A. V. Timonina, N. N. Kolesnikov, and E. V. Deviatov Phys. Rev. B 99, 125305 (2019)
- ³⁵ Qiunan Xu, Enke Liu, Wujun Shi, Lukas Muechler, Jacob Gayles, Claudia Felser, and Yan Sun PRB 97, 235416 (2018)
- ³⁶ A. M. Toxen Phys. Rev. 123, 442 (1961)
- ³⁷ P. Scharnhorst Phys. Rev. B 1, 4295 (1970).
- ³⁸ I. O. Kulik, Sov. Phys. JETP 30, 944 (1970).
- ³⁹ P. Dubos, H. Courtois, B. Pannetier, F. K. Wilhelm, A. D. Zaikin, and G. Schön Phys. Rev. B 63, 064502 (2001).
- ⁴⁰ J. C. Hammer, J. C. Cuevas, F. S. Bergeret, and W. Belzig, Phys. Rev. B 76, 064514 (2007).
- ⁴¹ A. Barone and G. Paterno, Physics and Applications of the Josephson Effect (John Wiley&Sons, New York, 1982).
- ⁴² Lin Jiao, Qiunan Xu, Yeryun Cheon, Yan Sun, Claudia Felser, Enke Liu, and Steffen Wirth Phys. Rev. B 99, 245158 (2019).
- ⁴³ F. S. Bergeret, A. F. Volkov, and K. B. Efetov, Phys. Rev. Lett. 86, 4096 (2001).
- ⁴⁴ F. S. Bergeret, A. F. Volkov, and K. B. Efetov, Rev. Mod. Phys. 77, 1321 (2005).
- ⁴⁵ R. S. Keizer, S. T. B. Goennenwein, T. M. Klapwijk, G. Miao, G. Xiao and A. Gupta, Nature 439, 825 (2006).
- ⁴⁶ A. I. Buzdin, Rev. Mod. Phys. 77, 935 (2005).
- ⁴⁷ F. S. Bergeret and I. V. Tokatly, Phys. Rev. Lett. 110, 117003 (2013).
- ⁴⁸ F. S. Bergeret and I. V. Tokatly, Phys. Rev. B 89, 134517 (2014).
- ⁴⁹ P. Dutta, F. Parhizgar, A.M. Black-Schaffer, arXiv:1911.04388